

“Reverse” Magnetostriction Effects in the [001] Shape Magnetostriction of $Ce_xLa_{1-x}Sb$ and $Sm_xLa_{1-x}Sb$ Single Crystals

G. J. Nieuwenhuys and D. Davidov

*Kamerlingh Onnes Laboratorium, Rijks Universiteit Leiden, Leiden, The Netherlands, and
Racah Institute of Physics, Hebrew University of Jerusalem, Jerusalem, Israel*

and

H. U. Häfner

*II. Physikalisches Institut, Universität zu Köln, Köln, Federal Republic of Germany
(Received 2 August 1982)*

Shape magnetostriction measurements along the [001] direction were carried out for all the magnetic rare-earth ions, R , in $R_xLa_{1-x}Sb$. At low temperatures the magnetostriction of both Ce and Sm are “reversed” with respect to the high temperatures. A crystal-field model can explain this phenomenon by the sign reversal of the expectation value of the quadrupole operator $\langle \hat{O}_2^0 \rangle$. The data are consistent with a negative second-order magnetoelastic coupling constant, V_2^3 , for all the rare-earth ions.

PACS numbers: 75.80.+q, 75.30.Et

Recently there has been extensive research on the magnetostriction of dilute rare-earth single crystals.¹⁻⁴ These measurements yield the lattice distortion produced by the quadrupole moment of the rare-earth ion via its interaction with the lattice modes.¹⁻⁴ In the first approximation the shape magnetostriction along the [001] direction is proportional therefore to the second-order magnetoelastic constant V_2^3 ,⁴ the Stevens factor α_J , and the expectation value of the rare-earth quadrupole operator $\langle \hat{O}_2^0 \rangle$ [$\hat{O}_2^0 = 3J_z^2 - J(J+1)$]. The magnetoelastic coupling constant, V_2^3 , is expected to retain its sign across the rare-earth series.^{1,2} The expectation value of \hat{O}_2^0 is always positive in the absence of crystalline-field effects, or for rare-earth ions in the second half of the rare-earth series even in the presence of crystalline field. Thus, for these rare-earth ions the shape magnetostriction reflects the sign of the Stevens factor α_J . This factor is related to the shape of the $4f$ charge distribution. Indeed, recent magnetostriction studies on $Ag:R$ and $Au:R$ (R stands for rare earth) single crystals^{1,2} with R belonging to the second half of the rare-earth series have confirmed this point: Namely, the magnetostriction follows the sign of α_J over the entire range of temperatures and applied fields.

This Letter reports new shape-magnetostriction measurement along the [001] direction performed on single crystals of $R_xLa_{1-x}Sb$ ($R = Ce, Pr, Nd, Sm, Tb, Dy, Ho, Er, Tm, \text{ and } Yb$) with emphasis on $Ce_xLa_{1-x}Sb$ and $Sm_xLa_{1-x}Sb$. All the rare-earth ions including Ce, Sm, and Yb exhibit well-defined local moments. To the best of

our knowledge, this work presents the first magnetostriction study on single crystals of dilute stable-valent rare-earth ions belonging to the first half of the rare-earth series. The most striking feature of our results is that the magnetostriction of $Ce_xLa_{1-x}Sb$ ($x \leq 0.15$) changes sign as a function of temperature; the “reverse magnetostriction” appears to be in conflict with the sign of the Stevens factor, α_J . Similar features have been observed for $Sm_xLa_{1-x}Sb$, but not for the rest of the $R_xLa_{1-x}Sb$ systems which exhibit a “normal magnetostriction” in the sense that the sign of the magnetostriction reflects the sign of α_J over the entire temperature range. The “anomalous” behavior of the reverse magnetostriction of $Ce_xLa_{1-x}Sb$ and $Sm_xLa_{1-x}Sb$ can be explained by a simple crystal-field theory. In fact we believe that our results clearly illustrate the importance of crystalline-field effects in the interpretation of any magnetostriction measurements.³

The magnetostriction was measured by the capacitance method in the temperature range between 1.5 and 40 K and applied external fields up to 5 T.³ The magnetic field was applied parallel to the measurement direction in all cases although a few measurements were carried out with the field applied perpendicular, to check for volume changes. Single crystals of $R_xLa_{1-x}Sb$ (NaCl cubic structure) of approximate dimensions of $3 \times 2 \times 2$ mm³ were used. For most of the rare-earth ions, measurements were carried out on two different crystals having different concentrations. This was necessary, especially for rare-earth systems exhibiting small magnetostriction, in

order to overcome any effects associated with unknown magnetic impurities in the 99.9+% "pure" lanthanum. For this reason we have restricted ourselves to rare-earth concentrations above 1%.

Figure 1 represents the magnetostriction of the "normal" Ho and Er substituted for the La in La Sb. These two cases are given as examples only for the purpose of comparison. Ho^{3+} ($\alpha_J < 0$) and Er^{3+} ($\alpha_J > 0$) exhibit Stevens coefficients which differ in sign; indeed the magnetostriction of these alloys (Fig. 1) has opposite signs. Similarly the magnetostriction of the alloys $R_x\text{La}_{1-x}\text{Sb}$ ($R = \text{Pr, Nd, Tb, Dy, Tm, Yb}$), which are not shown here, follows the sign of α_J . Exceptional cases are $\text{Ce}_x\text{La}_{1-x}\text{Sb}$ and $\text{Sm}_x\text{La}_{1-x}\text{Sb}$. One naively expects that, since α_J of Ce^{+3} has the same sign as that of Ho^{+3} , the low-temperature magnetostrictions should have the same signs. This is certainly not the case. Figure 2 exhibits the magnetostriction of $\text{Ce}_{0.15}\text{La}_{0.85}\text{Sb}$ as a function of external field and for various temperatures. Clearly, the magnetostriction of $\text{Ce}_{0.15}\text{La}_{0.85}\text{Sb}$, at low temperatures has an opposite sign to that of $\text{Ho}_{0.03}\text{La}_{0.97}\text{Sb}$. Furthermore, the magnetostriction of $\text{Sm}_x\text{La}_{1-x}\text{Sb}$ at low temperatures is also negative (note the Stevens factor in

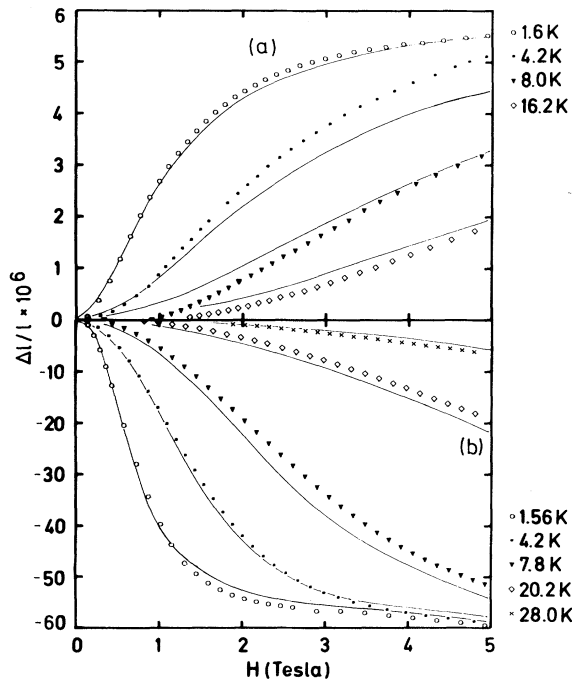


FIG. 1. Shape magnetostriction along the [001] direction of (a) $\text{Er}_{0.02}\text{La}_{0.98}\text{Sb}$ and (b) $\text{Ho}_{0.03}\text{La}_{0.97}\text{Sb}$. The solid lines are theoretical fits with the parameters given in Table I.

Table I) representing another example of reverse magnetostriction. No sign change of the magnetostriction was observed for the rest of the rare-earth systems tabulated in Table I.

Data were analyzed by the method developed by us recently.^{4,5} For shape magnetostriction along the [001] direction only the Γ_{3g} mode is important. Consequently, the total Hamiltonian describing the rare-earth ions as coupled to the Γ_{3g} lattice mode is given by

$$\hat{H} = \sum_i \hat{H}_{\text{ion}}^{(i)} + \sum_i \hat{H}_{\text{ion-lattice}}^{(i)} + \hat{H}_{\text{lattice}}, \quad (1)$$

where $H_{\text{ion}}^{(i)}$ is the ionic Hamiltonian which contains the Zeeman energy and the crystalline-field terms for a single ion i ,

$$\hat{H}_{\text{ion}}^{(i)} = g_J \mu_B \vec{H} \cdot \vec{J} + \beta_J A_4 \langle r^4 \rangle \hat{O}_4 + \gamma_J A_6 \langle r^6 \rangle \hat{O}_6. \quad (2)$$

Here g_J is the Landé g factor, μ_B is the Bohr magneton, \vec{H} is the external magnetic field, \hat{O}_4 and \hat{O}_6 are crystalline-field operators of the fourth and the sixth degree, respectively, and $A_4 \langle r^4 \rangle$ and $A_6 \langle r^6 \rangle$ are fourth-order and sixth-order crystalline-field parameters. The Hamiltonians H_{lattice} and $H_{\text{ion-lattice}}$ are given by

$$\hat{H}_{\text{lattice}} = \frac{1}{2} C(\Gamma_3) \epsilon^2(\Gamma_{3g\theta}) = \frac{1}{3} (C_{11} - C_{12}) \epsilon^2(\Gamma_{3g\theta}), \quad (3)$$

$$\hat{H}_{\text{ion-lattice}}^{(i)} = \frac{1}{3} \alpha_J V_2^3 \hat{O}_2^0 \epsilon(\Gamma_{3g\theta}), \quad (4)$$

where $C(\Gamma_3) = \frac{2}{3}(C_{11} - C_{12})$ is the elastic constant of force⁶ and $\epsilon(\Gamma_{3g\theta})$ is the normal strain defined as $\epsilon(\Gamma_{3g\theta}) = \frac{1}{2}(2\epsilon_{zz} - \epsilon_{xx} - \epsilon_{yy})$. Note that our model does not distinguish between microscopic and macroscopic strains.⁴ The net distortion $\langle \epsilon(\Gamma_{3g\theta}) \rangle$ can be calculated by use of the free energy de-

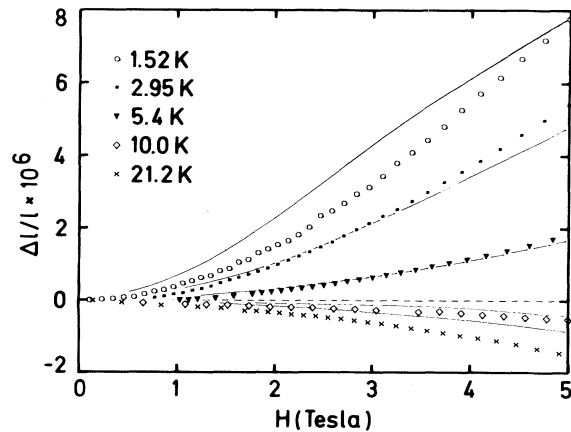


FIG. 2. Shape magnetostriction along [001] for $\text{Ce}_{0.15}\text{La}_{0.85}\text{Sb}$. The solid lines are fits to our theory with the parameters in Table I.

TABLE I. Experimental and theoretical parameters used in the fit of our model to the experimental [001] shape magnetostriction of $R_x \text{La}_{1-x} \text{Sb}$.

R	x^a	$A_4 \langle r^4 \rangle$ (K)	$A_6 \langle r^6 \rangle$ (K)	$10^2 \alpha_f$	$10^{-2} V_2^3$ (K)
Ce	0.15	18	...	-5.714	-17
Pr	0.1	81	4	-1.050	-130
Nd	0.03	88	4.5	-0.642	-85
Sm ^a	0.03	74	...	+4.126	-154
Tb	0.03	80	2.9	-1.010	-95
Dy	0.01	132	6.2	-0.6371	-92
Ho	0.03	90	16	-0.2222	-95
Er	0.02	80	2.2	+0.2539	-64
Tm	0.1	86	3.0	+1.010	-104
Yb	0.05	75	8	0.3746	-44

^a x denotes R concentration. All the concentrations are nominal. For rare-earth ions Er and Dy (for which magnetostriction as a function of concentration was studied), the magnetostriction scales with the nominal concentration. For the case of $\text{Sm}_x \text{La}_{1-x} \text{Sb}$, the two samples measured (i.e., 3% and 10% nominal) yield different magnetostrictions which do not scale with concentration. The reverse magnetostriction, however, was observed in both samples. The value of V_2^3 for $\text{Sm}_x \text{La}_{1-x} \text{Sb}$ should be regarded therefore with caution.

finied as^{4,5}

$$F = k_B T \ln \sum_i \exp(-E_i / k_B T), \quad (5)$$

where $\{E_i\}$ are eigenvalues of (1). These eigenvalues can be calculated by a complete diagonalization of (1) provided that the crystalline-field parameters and the elastic and magnetoelastic constants, as well as \vec{H} and T , are all known. Knowledge of E_i , with $\epsilon(\Gamma_{3g\theta})$ as an unknown parameter, enables one to calculate the free energy $F(\epsilon)$ as a function of ϵ [$\epsilon \equiv \epsilon(\Gamma_{3g\theta})$]. As has been demonstrated previously,⁴ $F(\epsilon)$ exhibits a minimum which yields the most stable distortion $\langle \epsilon \rangle$. This theoretical distortion is compared with the experiment.

In our fitting procedure we have adapted the value of the elastic constant of force for LaSb from the work of Mullen *et al.*^{4,6,7} to be $C(\Gamma_3) = 420,000$ K/ion. This is not completely justified, and the presence of rare-earth impurities certainly modifies $C(\Gamma_3)$.⁶ As starting values for the crystalline-field parameters we have used the values of Davidov *et al.*,⁸ Birgeneau *et al.*,⁹ and Mullen *et al.*⁶ for rare-earth antimonides. The best fits of the theoretical distortion to the experimental distortion yield the experimental parameters V_2^3 , $A_4 \langle r^4 \rangle$, and $A_6 \langle r^6 \rangle$. The solid lines in Fig. 1 rep-

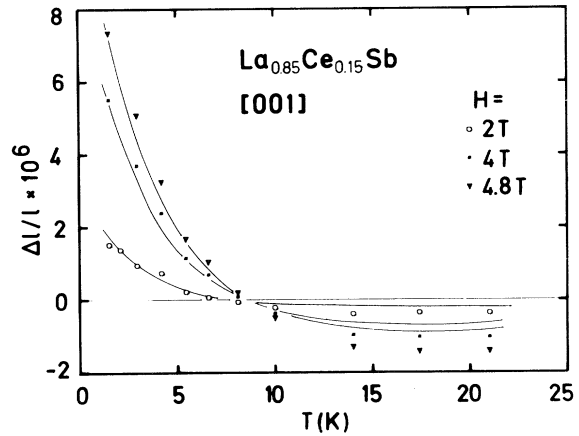


FIG. 3. Temperature dependence of $\Delta L/L$ at various magnetic fields. Note that $\Delta L/L$ is roughly related to $\langle \hat{O}_2^0 \rangle$. Solid lines are theoretical fits.

resent the best fit achieved for the case of $\text{Ho}_{0.03} - \text{La}_{0.97} \text{Sb}$ and $\text{Er}_{0.02} \text{La}_{0.98} \text{Sb}$ with the parameters given in Table I. As is clearly seen the fit is good. The same quality of theoretical fit to the experiment was observed for the systems $R_x - \text{La}_{1-x} \text{Sb}$ ($R = \text{Pr}, \text{Nd}, \text{Dy}, \text{Ho}, \text{Er}, \text{Yb}$) with the parameters given in Table I. For the rare-earth ion Ce, Sm, Tb, and Tm the agreement is not as good (see Fig. 2 for the case of $\text{Ce}_{0.15} \text{La}_{0.85} \text{Sb}$), probably because of interaction effects in these more concentrated systems.⁴

The most striking feature of our results in Table I is that V_2^3 retains its sign across the rare-earth series. It is always negative and has roughly the same order of magnitude (except for the low value for Ce) for all the rare-earth ions in LaSb. The negative sign of V_2^3 is consistent with the prediction of the point-charge model.⁶ Also the crystalline-field parameter $A_4 \langle r^4 \rangle$ does not vary significantly (except the case of Ce) across the series and roughly agrees with the crystalline-field parameter found previously for the concentrated antimonides⁹ and the dilute antimonides.⁸

In the framework of our model, the sign change of the magnetostriction of $\text{Ce}_{0.15} \text{La}_{0.85} \text{Sb}$ and the reverse magnetostriction are attributed to the properties of the quadrupole operator $\langle \hat{O}_2^0 \rangle$ in this system. Our theoretical fits yield an overall crystalline-field splitting of 42 K between the Γ_7 ground state and the Γ_8 excited state of Ce in LaSb. Thus, at low temperatures the induced quadrupole moment is due to admixture with the Γ_8 excited state (as $\langle \Gamma_7 | \hat{O}_2^0 | \Gamma_7 \rangle = 0$). The matrix elements of admixture for the case of Ce^{+3} are negative leading to a negative value for $\langle \hat{O}_2^0 \rangle$ at

low temperatures. At higher temperatures the Γ_8 is populated, giving rise to a positive contribution $\langle \Gamma_8 | \hat{O}_2^0 | \Gamma_8 \rangle$. The temperature variation of the magnetostriction for various magnetic fields is shown in Fig. 3. Our ability to observe the sign reversal of $\langle \hat{O}_2^0 \rangle$ might be important for the interpretation of the complicated phase diagram observed in concentrated Ce systems and particularly in CeSb.¹⁰ This is because quadrupole-quadrupole interactions are probably important and partially responsible for these complicated structural-magnetic phase transitions. To the best of our knowledge this sign reversal of $\langle \hat{O}_2^0 \rangle$ was never taken into consideration.

We would like to thank V. Shigarodsky for making most of the single crystals in this work, and Professor D. Wohlleben and J. Mydosh for critical reading of the manuscript and for discussions. This work was supported by Fundamenteel Onderzoek der Materie, Holland, and by Sonderforschungsbereich 125, Deutsche Forschungsgemeinschaft.

¹G. Creuzet and I. A. Campbell, Phys. Rev. B 23, 3375 (1981); I. A. Campbell, G. Creuzet, and J. San-

chez, Phys. Rev. Lett. 43, 234 (1979).

²G. Creuzet and I. A. Campbell, J. Magn. Magn. Mater. 27, 221 (1982).

³K. Nicholson, H. U. Häfner, E. Müller-Hartmann, and D. Wohlleben, Phys. Rev. Lett. 41, 1325 (1978); H. U. Häfner, H. W. Ludwigs, K. Nicholson, and D. Wohlleben, Z. Phys. B 42, 219 (1981).

⁴G. J. Nieuwenhuys, D. Davidov, H. U. Häfner, and M. J. Bloch, Solid State Commun. 43, 51 (1982).

⁵M. J. Bloch and D. Davidov, Phys. Rev. B, to be published.

⁶M. E. Mullen, B. Lüthi, P. S. Wang, E. Bucher, L. D. Longinotti, and J. P. Maita, Phys. Rev. B 10, 186 (1974).

⁷M. J. Bloch, D. Davidov, and C. Rettori, J. Magn. Magn. Mater. 25, 271 (1982).

⁸D. Davidov, E. Bucher, L. W. Rupp, Jr., L. D. Longinotti, and C. Rettori, Phys. Rev. B 9, 2879 (1974).

⁹R. J. Birgeneau, E. Bucher, L. Passell, and K. C. Turberfield, Phys. Rev. B 4, 718 (1971); K. C. Turberfield, L. Passell, R. J. Birgeneau, and E. Bucher, J. Appl. Phys. 42, 1746 (1971).

¹⁰J. Rossat-Mignod *et al.*, Phys. Rev. B 16, 440 (1977); B. R. Cooper and R. Siegmann, J. Appl. Phys. 50, 1991 (1979); B. R. Cooper, Phys. Rev. 17, 293 (1978); P. Fischer, B. Lebeck, G. Meier, B. D. Rainford, and O. Vogt, J. Phys. 11, 345 (1978).